Proceedings of the 11th Brazilian Congress of Thermal Sciences and Engineering -- ENCIT 2006
Braz. Soc. of Mechanical Sciences and Engineering -- ABCM, Curitiba, Brazil,- Dec. 5-8, 2006

Paper CIT06-0474

MESH TOPOLOGY INFLUENCE ON SUPERSONIC BLUNT BODY FLOW SOLUTIONS

Fábio Rodrigues Guzzo
CTA/ITA – Instituto Tecnológico de Aeronáutica
fabio@guzzo.com.br

João Luiz F. Azevedo
CTA/IAE – Instituto de Aeronáutica e Espaço
azevedo@iae.cta.br

Abstract. *The present work is concerned with studying the mesh topology influence on supersonic blunt body flow numerical solutions. The work is motivated by previous difficulties the authors experienced when trying to compute very high speed flows with chemical reactions over blunt bodies. Some test cases led to property oscillations, rendering, solutions without physical meaning, in a chemically reacting mixture flow context. Recently, however, the authors observed that the regularity and the smoothness of the computational meshes have a very positive effect on the quality of the solutions obtained for such cases. Hence, in this context, the work here reported considers the solutions of axisymmetric flows over blunt bodies using three different mesh topologies: triangular and quadrilateral unstructured grids and quadrilateral structured grids. The flowfields of interest are modeled by the axisymmetric Euler equations, and ideal gases are considered. The flow equations are solved by a cell centered finite volume method, in which Liou's AUSM+ flux-vector splitting scheme is used for flux computations at cell interfaces. Time march uses a fully explicit, 5-stage, Runge-Kutta time stepping scheme. The numerical methodology employed has performed considerably better for the quadrilateral grids and for the structured meshes, in opposition to the triangular grid and the unstructured meshes, respectively.*

Keywords. *CFD, Mesh Influence, Blunt Body Flow Solutions, AUSM+ scheme.*

1. Introduction

Unstructured meshes, specifically triangular grids in 2-D or tetrahedral grids in 3-D, are preferable when treating complex geometries, and have received considerable attention of the Computational Fluid Dynamic (CFD) community in the past few years. Due to the geometric flexibility and the availability of well-defined algorithms for good-quality mesh generation, general grid generation and remeshing adaptation are easier to conceive for unstructured meshes composed by triangular elements. However, it is important to mention that general systems that incorporate the possibility for generating and remeshing quadrilateral and hybrid meshes over arbitrary domains are feasible. Lyra *et al*. (2000) describe the main features of an integrated computational system for automatic two-dimensional mesh generation and remeshing adaptation for triangular, quadrilateral or mixed meshes.

The present work is concerned with the study of the mesh topology influence over the quality of supersonic blunt body CFD solutions. One unstructured triangular grid, one unstructured quadrilateral grid and two structured quadrilateral grids are considered. It is known that certain formulations perform better with quadrilateral elements than with triangular elements (Lyra *et al*., 2000). The numerical code used herein was already validated by Strauss and Azevedo (2001).

The governing formulation employed comprises the dimensionless, axisymmetric Euler equations. The constitutive relation is the ideal gas equation. Specific heats, at constant volume and pressure, are assumed to be constant. The spatial discretization is performed in a cell centered, face-based finite volume procedure on unstructured meshes. An upwind scheme, AUSM+ (Advection Upstream Splitting Method), proposed by Liou (1994; 1996) for structured meshes, is used. The reinterpretation of the formulation for unstructured meshes follows Azevedo and Korzenowski (1998). Boundary conditions are set through the use of ghost cells attached to the boundary faces. A fully explicit, second order accurate, five stage Runge-Kutta method was used as the time-stepping scheme. Since the problem of interest is steady state, a local time stepping option has been implemented, *i.e.*, the CFL number is kept constant throughout the field.

The configuration studied is a supersonic flow over a semi-spherical blunt body. Four solutions for this configuration are generated using different meshes, one for triangular unstructured grid, one for quadrilateral unstructured grid and two for structured quadrilateral grids. The solutions are presented, compared and discussed.

2. Theoretical Formulation

The flow is modeled by the dimensionless azimuthal-invariant Euler equations in cylindrical coordinates. Perfect gas and constant specific heat, at constant volume and pressure, are considered. The equations employed are written as

$$\frac{\partial \mathbf{Q}}{\partial t}+\frac{\partial \mathbf{E}r}{\partial z}+\frac{\partial \mathbf{F}r}{\partial r}+\mathbf{H}=0. \tag{1}$$

The vector of conserved variables, $\mathbf{Q}$, the convective flux vectors, $\mathbf{E}$ and $\mathbf{F}$, and the axisymmetry source term, $\mathbf{H}$, are given by

$$\mathbf{Q}=\begin{bmatrix}\rho\\ \rho u_z\\ \rho u_r\\ \rho e\end{bmatrix},\quad \mathbf{E}=\begin{bmatrix}\rho u_z\\ \rho u_z^2+p\\ \rho u_z u_r\\ u_z(\rho e+p)\end{bmatrix},\quad \mathbf{F}=\begin{bmatrix}\rho u_r\\ \rho u_z u_r\\ \rho u_r^2+p\\ u_r(\rho e+p)\end{bmatrix},\quad \mathbf{H}=\begin{bmatrix}0\\ 0\\ -p/r\\ 0\end{bmatrix}. \tag{2}$$

The nomenclature used herein is the standard one, such that ρ is the density, u_z and u_r are the velocity components, e is the total energy per unit of mass and p is the pressure. Equation (1) is supplemented by the following constitutive equation:

$$p=(\gamma-1)\rho\left[e-\frac{1}{2}\left(u_z^2+u_r^2\right)\right], \tag{3}$$

where γ is the ratio of specific heats. γ equals to 1.4 was assumed. In this work, the properties are made dimensionless according to the following equations

$$t=t_d\frac{a_\infty}{l_0},\ z=\frac{z_d}{l_0}, r=\frac{r_d}{l_0}\ ,\ u_z=\frac{u_{zd}}{a_\infty},\ ur=\frac{u_{rd}}{a_\infty},\ p=\frac{p_d}{\rho_\infty a_\infty^2},\ e=\frac{e_d}{a_\infty^2}. \tag{4}$$

The subscript d denotes the dimension properties. l_0 is the reference length, a_∞ is the freestream speed of sound and ρ_∞ is the freestream density.

3. Numerical Formulation

The governing equations are discretized in a stationary mesh. Finite volume cell centered method is employed. The formulation is obtained by integrating the equations in each finite volume and assuming that the convective flux vectors, $\mathbf{E}$ and $\mathbf{F}$, are constant in each face of the control volume. The equations employed at each cell are written as

$$\frac{\partial \mathbf{Q}_i}{\partial t}+\frac{1}{Vi}\left[\sum_{k=1}^{nf}\left(\mathbf{E}_{ik}r_{ik}\Delta r_{ik}-\mathbf{F}_{ik}r_{ik}\Delta z_{ik}\right)+\mathbf{D}(\mathbf{Q}_i)\right]+\mathbf{H}_i=0. \tag{5}$$

Here, nf is the number of neighboring cells of the i-th cell and $\mathbf{D}(\mathbf{Q}_i)$ is the artificial dissipation operator. The subscript ik denotes the property values at the interface between the i-th cell and its k-th neighbor. r_{ik} was defined as the average r at the interface. A scheme of the edge nomenclature of the *ik* interface is presented in the Fig. 1. The discrete value of the vector of conserved variables for the i-th cell, $\mathbf{Q}_i$, and of the axisymmetry source term, $\mathbf{H}_i$, are defined as the mean value of the continuous properties in the volume. The summation term of the Eq. (5), $\sum_{k=1}^{nf}\left(\mathbf{E}_{ik}r_{ik}\Delta r_{ik}-\mathbf{F}_{ik}r_{ik}\Delta z_{ik}\right)$, is also called as the convective operator, $\mathbf{C}(\mathbf{Q}_i)$:

$$\mathbf{C}(\mathbf{Q}_i)=\sum_{k=1}^{nf}\left(\mathbf{E}_{ik}r_{ik}\Delta r_{ik}-\mathbf{F}_{ik}r_{ik}\Delta z_{ik}\right). \tag{6}$$

An upwind scheme, AUSM+ (Advection Upstream Splitting Method), proposed by Liou (1994; 1996), was used. $\mathbf{E}$ and $\mathbf{F}$ can be expressed as a sum of the convective and pressure terms:

$$\mathbf{E}=u_z\mathbf{\Phi}+\mathbf{P}_z=M_z a\mathbf{\Phi}+\mathbf{P}_z, \tag{7}$$

$$\mathbf{F}=u_r\mathbf{\Phi}+\mathbf{P}_r=M_r a\mathbf{\Phi}+\mathbf{P}_r, \tag{8}$$

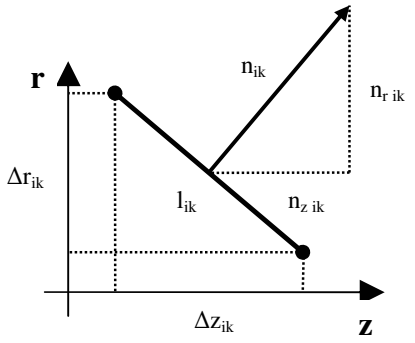

Figure 1. Edge Nomenclature.

where $\mathbf{\Phi}$, $\mathbf{P}_z$, $\mathbf{P}_r$ vectors are defined as

$$\mathbf{\Phi} = \begin{bmatrix} \rho \\ \rho u_z \\ \rho u_r \\ (\rho e + p) \end{bmatrix}, \ \mathbf{P}_z = \begin{bmatrix} 0 \\ p \\ 0 \\ 0 \end{bmatrix}, \ \mathbf{P}_r = \begin{bmatrix} 0 \\ 0 \\ p \\ 0 \end{bmatrix}. \tag{9}$$

In these expressions, a is the speed of sound, $M_z = u_z / a$ and $M_r = u_r / a$. The term $\mathbf{E}_{ik} r_{ik} \Delta r_{ik} - \mathbf{F}_{ik} r_{ik} \Delta z_{ik}$ of the Eq. (6) can be then written as

$$\mathbf{E}_{ik} r_{ik} \Delta r_{ik} - \mathbf{F}_{ik} r_{ik} \Delta z_{ik} = \left(\mathbf{F}_{ik}^{(c)} + \mathbf{P}_{ik} \right) r_{ik} l_{ik}, \tag{10}$$

where the vectors $\mathbf{F}_{ik}^{(c)}$ and $\mathbf{P}_{ik}$ are defined as

$$\mathbf{F}_{ik}^{(c)} = \left(u_{z\,ik} n_{z\,ik} \mathbf{\Phi}_{ik} + u_{r\,ik} n_{r\,ik} \mathbf{\Phi}_{ik} \right), \tag{11}$$

$$\mathbf{P}_{ik} = \left(\mathbf{P}_{z\,ik} n_{z\,ik} + \mathbf{P}_{r\,ik} n_{r\,ik} \right). \tag{12}$$

The approach adopted in the present work in order to extend the formulation proposed by Liou (1994; 1996) to unstructured meshes follows Azevedo and Korzenowski (1998) and consists in defining a local one-dimensional system normal to the edge considered. Azevedo and Korzenowski (1998) describe the method to calculate the terms $\mathbf{F}_{ik}^{(c)}$ and $\mathbf{P}_{ik}$ for unstructured meshes. The upwind scheme used herein, AUSM+, does not require the use of additional artificial dissipation in order to control nonlinear instabilities. However, it was introduced in some simulations to analyze and to propose a feasible way to reduce flow oscillations in the field. The artificial dissipation operator, $\mathbf{D}(\mathbf{Q}_i)$, used in the present work, is formed as a blend of undivided Laplacian and biharmonic operators (Jameson and Mavriplis, 1986 and Mavriplis, 1988, 1990). These mimic, in an unstructured mesh context, the concept of using 2nd and 4th difference terms as presented by Jameson *et al.* (1981) and Pulliam (1986). The artificial dissipation is written as

$$\mathbf{D}(\mathbf{Q}_i) = \mathbf{d}^{(2)}(\mathbf{Q}_i) - \mathbf{d}^{(4)}(\mathbf{Q}_i), \tag{13}$$

where $\mathbf{d}^{(2)}(\mathbf{Q}_i)$ represents the contribution of the undivided Laplacian operator, and $\mathbf{d}^{(4)}(\mathbf{Q}_i)$ the contribution of the biharmonic operator. The undivided Laplacian artificial dissipation operator and the biharmonic operator are described by Jameson and Mavriplis, (1986) and Mavriplis, (1988, 1990). The parameters used to adjust the artificial dissipation, i.e. $K^{(2)}$ and $K^{(4)}$, received here the greatest values within the ranges suggested by Jameson *et al.* (1981) and Mavriplis (1990).

The fully explicit, 5-stage, Runge-Kutta method was used as the time-stepping scheme. The time integration for the i-th cell is expressed as

$$
\begin{aligned}
&\mathbf{Q}_i^{(0)} = \mathbf{Q}_i^n, \\
&\mathbf{Q}_i^{(1)} = \mathbf{Q}_i^{(0)} - \alpha_1 \Delta t_i^n \left[\frac{1}{V_i} \left[\mathbf{C}\left(\mathbf{Q}_i^{(0)}\right) - \mathbf{D}\left(\mathbf{Q}_i^{(0)}\right) \right] + \mathbf{H}_i^{(0)} \right], \\
&\mathbf{Q}_i^{(2)} = \mathbf{Q}_i^{(0)} - \alpha_2 \Delta t_i^n \left[\frac{1}{V_i} \left[\mathbf{C}\left(\mathbf{Q}_i^{(1)}\right) - \mathbf{D}\left(\mathbf{Q}_i^{(1)}\right) \right] + \mathbf{H}_i^{(1)} \right], \\
&\mathbf{Q}_i^{(3)} = \mathbf{Q}_i^{(0)} - \alpha_3 \Delta t_i^n \left[\frac{1}{V_i} \left[\mathbf{C}\left(\mathbf{Q}_i^{(2)}\right) - \mathbf{D}\left(\mathbf{Q}_i^{(1)}\right) \right] + \mathbf{H}_i^{(2)} \right], \\
&\mathbf{Q}_i^{(4)} = \mathbf{Q}_i^{(0)} - \alpha_4 \Delta t_i^n \left[\frac{1}{V_i} \left[\mathbf{C}\left(\mathbf{Q}_i^{(3)}\right) - \mathbf{D}\left(\mathbf{Q}_i^{(1)}\right) \right] + \mathbf{H}_i^{(3)} \right], \\
&\mathbf{Q}_i^{(5)} = \mathbf{Q}_i^{(0)} - \alpha_5 \Delta t_i^n \left[\frac{1}{V_i} \left[\mathbf{C}\left(\mathbf{Q}_i^{(4)}\right) - \mathbf{D}\left(\mathbf{Q}_i^{(1)}\right) \right] + \mathbf{H}_i^{(4)} \right], \\
&\mathbf{Q}_i^{n+1} = \mathbf{Q}_i^{(5)}.
\end{aligned}
\tag{14}
$$

The superscript n and $n+1$ refer to the states at the beginning and at the end of a generic n-th time step. The artificial dissipation operator, $\mathbf{D}(\mathbf{Q}_i)$, is evaluated only at the two initial stages is order to reduce timing process. The values used for the α coefficients are

$$
\alpha_1 = \frac{1}{4},\ \alpha_2 = \frac{1}{6},\ \alpha_3 = \frac{3}{8},\ \alpha_4 = \frac{1}{2},\ \alpha_5 = 1. \tag{15}
$$

These values were suggested by Mavriplis (1988; 1990). A specific time stepping value is determined for each i-th cell, Δt_i^n, as

$$
\Delta t_i^n = \frac{(CFL)(\Delta s_i)}{\left(\sqrt{u_z^2 + u_r^2} + a\right)_i^n}. \tag{16}
$$

A constant CFL number was used and attributed throughout the field. (Δs_i) is the characteristic length associated to the i-th cell, and it has been defined as the diameter of the inscribed circle of the element. a is the local speed of sound.

Boundary conditions are set through the use of ghost cells attached to the boundary faces. The flow is made tangent at the wall boundary by imposing the velocity component normal to the wall, in the ghost volume, the same magnitude value and opposite sign of the normal velocity component in its adjacent interior volume, whereas the ghost volume velocity component tangent to the wall is equal in magnitude and sign to its internal volume counterpart. Zero normal pressure and temperature gradients are assumed at the wall. Symmetry boundary is modeled as the wall boundary. The variables in the ghost volumes at the entrance boundary are set equal to the freestream values. For the exit boundary, all properties are extrapolated from the interior information, i.e. the variables of the ghost volume are made equal to the variables of its interior volume counterpart. Initial condition is set by applying the freestream properties over each cell.

4. Results and Discussion

4.1 Supersonic Flow over a Blunt Body

The configuration studied is a supersonic flow over a semi-spherical blunt body. Freestream Mach number equal to 4 and zero flow angle of attack are considered. This configuration was selected because flows over blunt bodies with detached shock waves are widely explored in the literature and their comprehensive study has become important with the advent of ballistic missiles and, specially, reentry vehicles. Artificial dissipation terms are not considered in the simulations here presented. These terms are used in the additional solutions, discussed in the next section, in order to analyze their effects on the reduction of property oscillations. Four simulations are performed and the solutions are herein presented: one for triangular unstructured grid, one for quadrilateral unstructured grid, and two for structured quadrilateral grids. Figure 2 shows the meshes employed. The triangular unstructured mesh is composed of 13456 nodes and 26408 volumes; the quadrilateral unstructured mesh comprises 26939 nodes and 26508 volumes; the quadrilateral structured mesh 1, which is the fine structured mesh, has 18000 nodes and 17641 volumes, in which the distribution is 60 × 300 points in the normal and longitudinal directions, respectively; and the quadrilateral structured mesh 2, which is the coarse structured mesh, has 4500 nodes and 4321 volumes, distributed as 30 × 150 points in the

normal and longitudinal directions. The number of volumes that composes both structured meshes is considerably lower than the number of volumes of the unstructured meshes. The quadrilateral structured mesh 2 has the greatest local mesh spacing throughout the field, even near the symmetry boundary. This mesh was included in order to assure that the analysis presented here is restricted to the mesh topology and the effects are not due to the mesh refinement. The unstructured meshes were generated with ICEM CFD code. The grids were smoothed using the quality criteria (ICEM CFD, 1999). A single mesh spacing was considered through out the field. For the structured meshes, the nodes are equally spaced in the normal and longitudinal directions. In order to assess the qualities of the meshes, Fig. 3 shows details of each mesh, upstream of the body stagnation point, and Fig. 4 shows the angle distribution of the elements of the meshes.

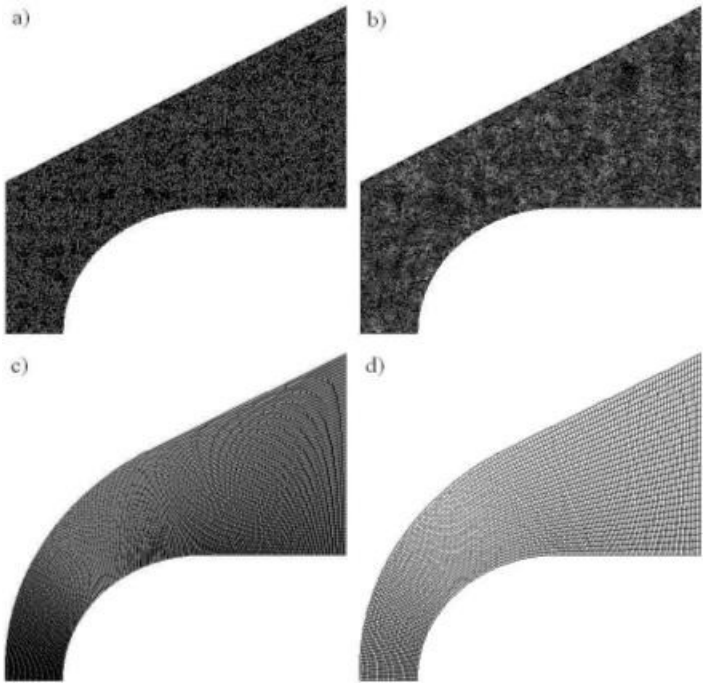

Figure 2. Computational meshes: a) triangular unstructured grid, b) quadrilateral unstructured grid, c) quadrilateral structured grid 1 and d) quadrilateral structured grid 2 .

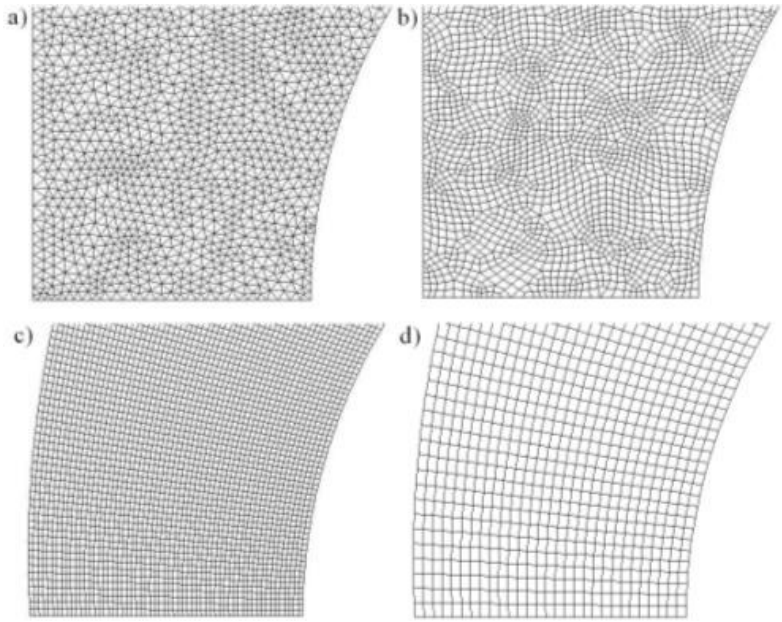

Figure 3. Detailed view of the upstream region of the various meshes: a) triangular unstructured grid, b) quadrilateral unstructured grid, c) quadrilateral structured grid 1 and d) quadrilateral structured grid 2.

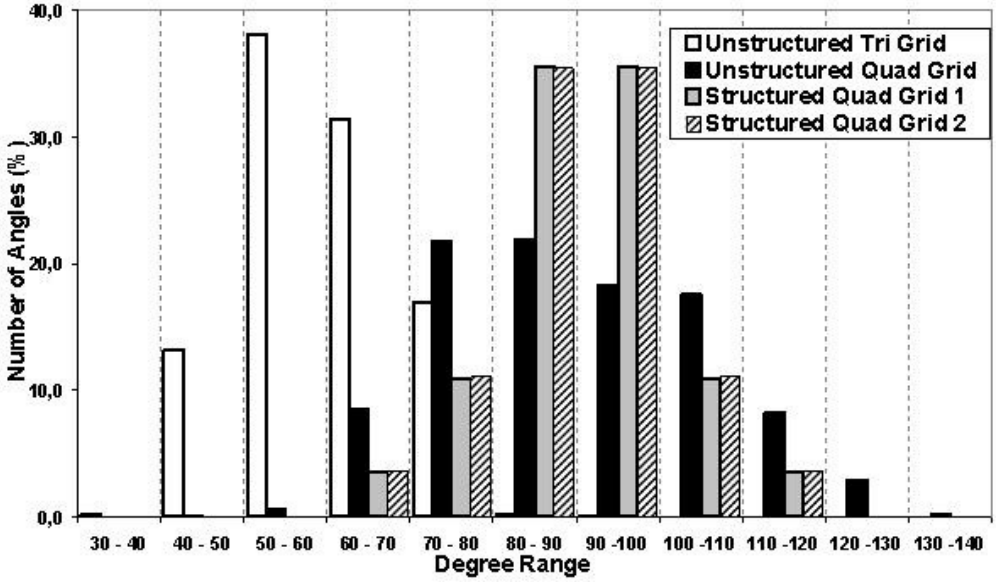

Figure 4. Angle distributions for the various meshes.

Figure 5 shows the density, ρ, and the Mach number, M, contours of the simulations performed using each of the meshes considered. All solutions presented herein are converged. It is possible to note that, although the property contours after the shock wave are similar among the solutions, oscillations of ρ and M are more pronounced for the triangular grid solution in comparison with the quadrilateral grid solutions. Moreover, the same statement can be made for the unstructured mesh results in comparison with the structured mesh calculations. Property oscillations are more perceptive in the solution obtained with the triangular unstructured mesh compared to the quadrilateral unstructured mesh, especially for Mach number, after the region where the variation of the properties is more severe, *i.e.*, after the shock wave and near the symmetry boundary. The solution obtained for the quadrilateral structured meshes presented considerable less oscillation compared to the unstructured meshes, both for density and for Mach number.

Figure 6 shows the contours of constant $M = 3.9$. Since the shock wave in a numerical simulation is not a discontinuity in the solution, the determination of its real position has a certain subjectivity. The contour of constant M equal to 3.9 is considered as the approximate shock wave position because it is simple to compute and it allows consistent comparisons. Although oscillations of the properties are observed, mainly in the solution for the unstructured meshes, as already shown in Fig. 5, differences of the shock wave position are not pronounced among the solutions obtained, as shown in Fig. 6.

Figure 7 shows the pressure distributions along the symmetry and wall boundaries. Oscillations are more perceptive in the solutions obtained with the unstructured meshes in comparison with the structured meshes, as already evidenced in Figs. 5 and 6. Despite the oscillations, the pressure distributions, in the region after the shock wave, are similar for the four simulations. The differences of the shock wave position are not pronounced among the solutions obtained, as also observed in Fig. 6.

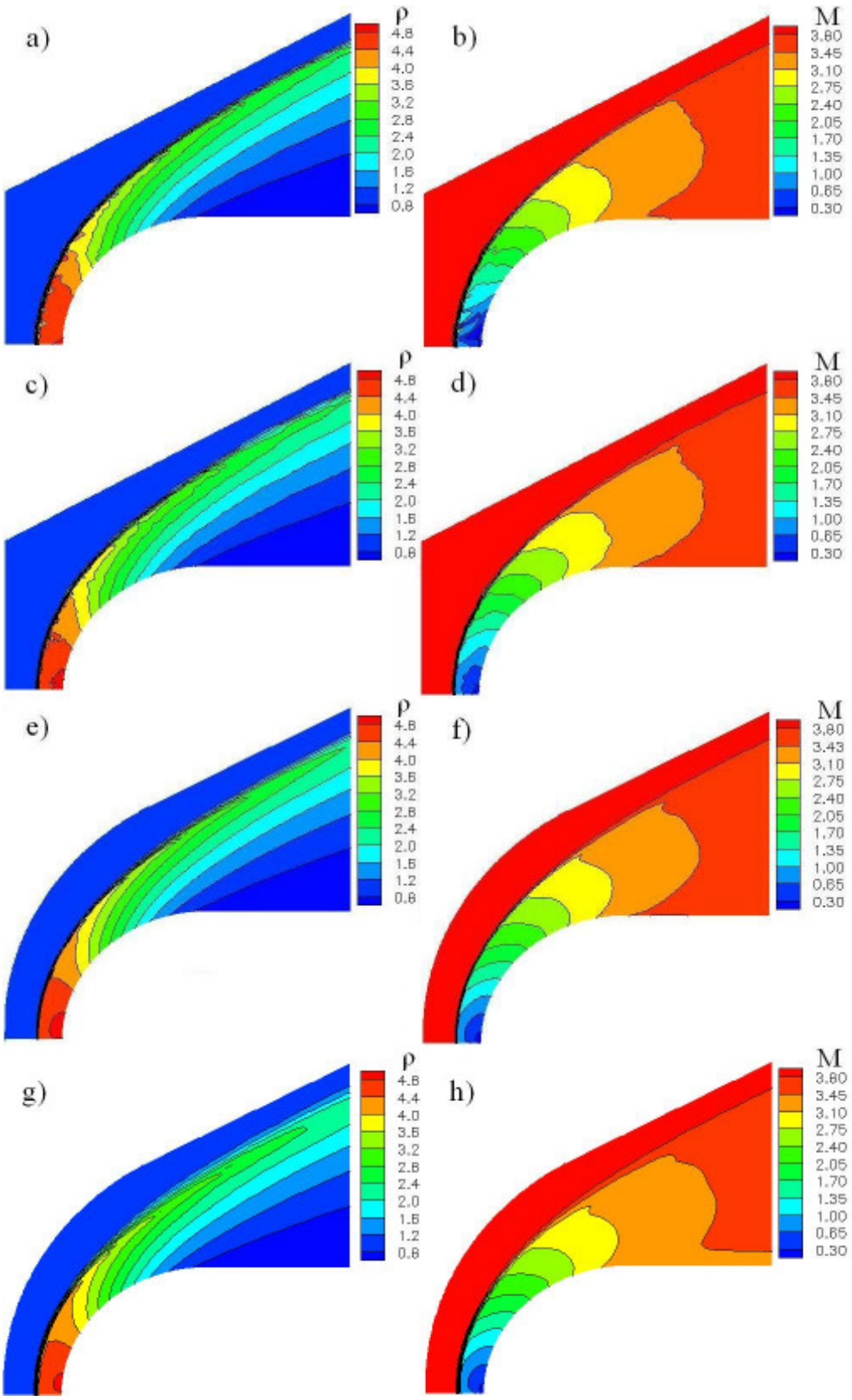

Figure 5. Density, ρ, and Mach number, M, contours: a) and b) for triangular unstructured mesh, c) and d) for quadrilateral unstructured mesh, e) and f) for quadrilateral structured mesh 1, and g) and h) for quadrilateral structured mesh 2. $M_\infty = 4$, zero angle of attack and no artificial dissipation.

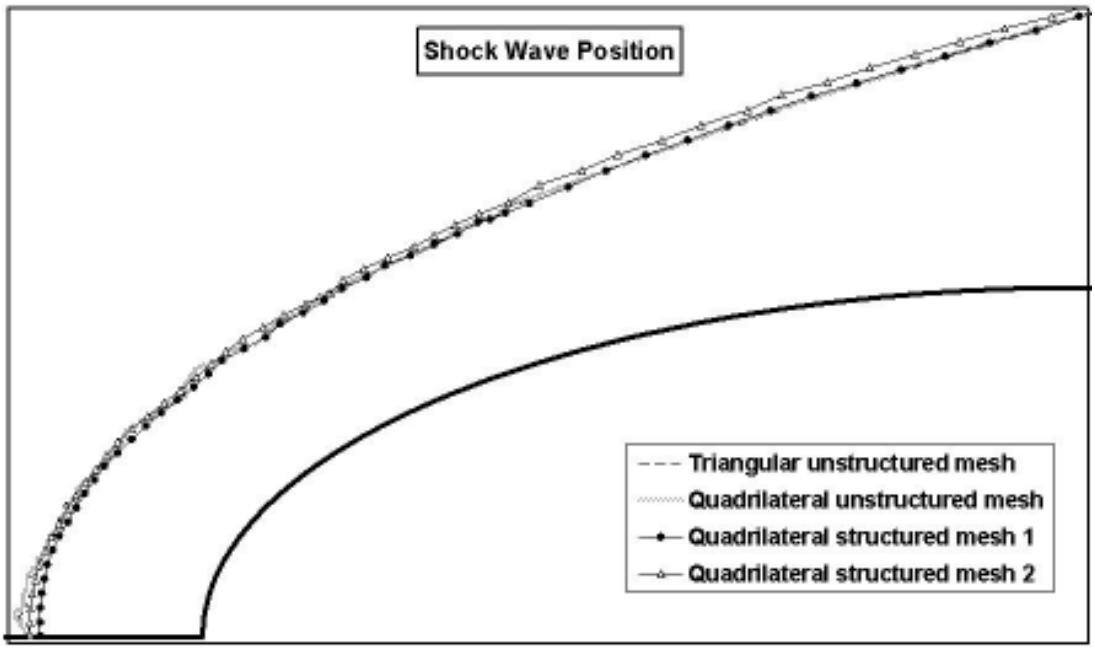

Figure 6. Shock wave position of the simulations performed: contours of constant $M = 3.9$. $M_\infty = 4$, zero angle of attack and no artificial dissipation.

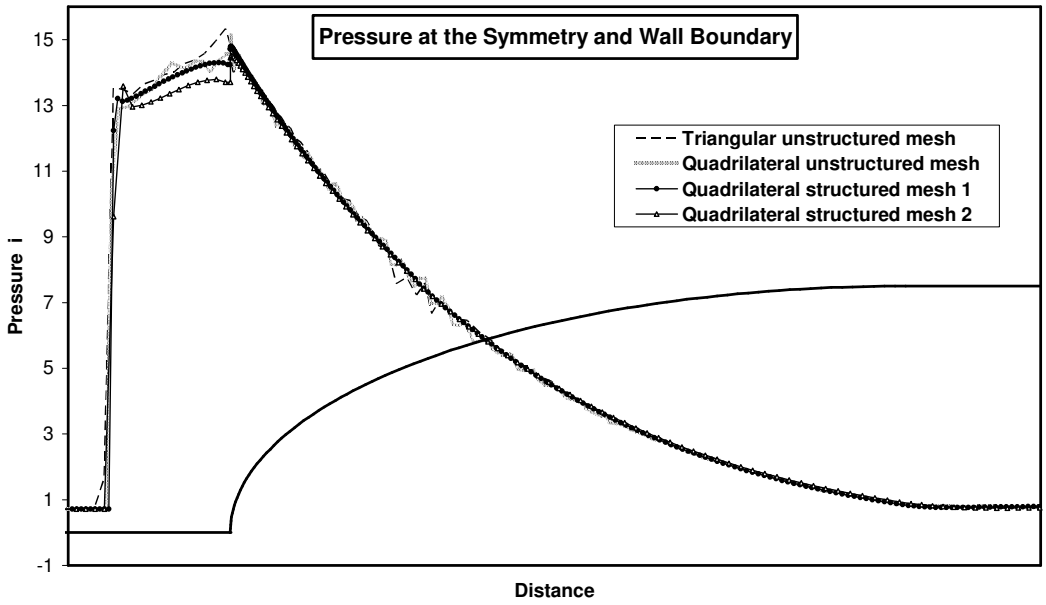

Figure 7. Pressure distributions along the symmetry and wall boundaries. $M_\infty = 4$ and no artificial dissipation.

4.2 Additional Results

Additional solutions are presented here in order to extend the analysis of the mesh topology influence. Simulations are performed over a configuration identical to the previous one, except that the freestream Mach number is equal to 5. Figure 8 shows the density, ρ, and Mach number, M, contours for the meshes considered. Artificial recirculation is observed over the triangular unstructured mesh after the shock wave, near the symmetry boundary. The property oscillations over the field may be led to this artificial recirculation. This solution is not converged and it differs considerably from the solutions obtained for the quadrilateral meshes. Figure 9 shows details of the artificial recirculation observed over the triangular unstructured mesh.

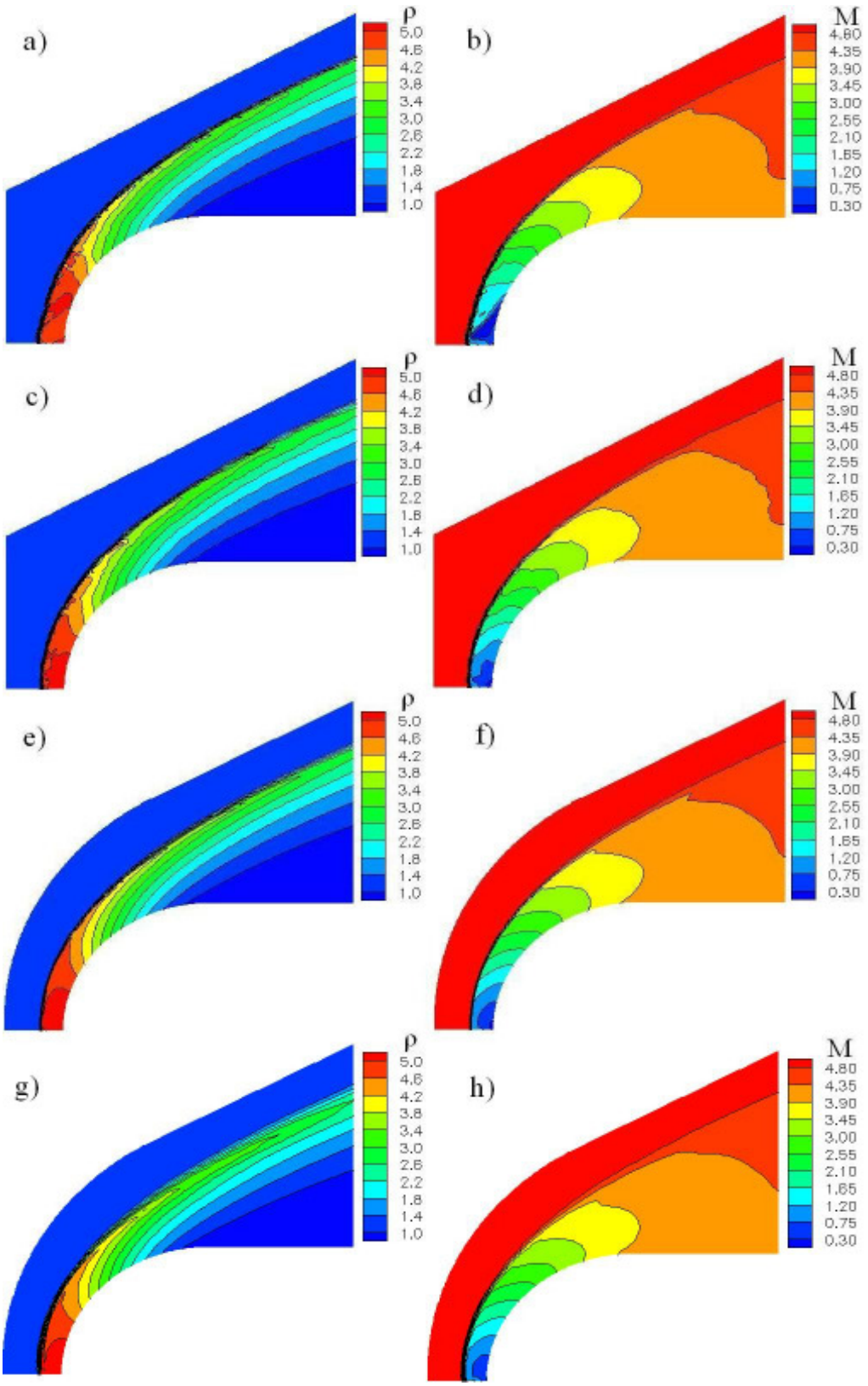

Figure 8. Density, ρ, and Mach number, M, contours: a) and b) for triangular unstructured mesh, c) and d) for quadrilateral unstructured mesh, e) and f) for quadrilateral structured mesh 1, and g) and h) for quadrilateral structured mesh 2. $M_\infty = 5$ and no artificial dissipation.

The property oscillations observed in the simulations performed with the unstructured meshes, shown in the Fig. 8, are considerably reduced and the appearance of artificial recirculation in the solution over the triangular unstructured mesh is eliminated with the use of additional artificial dissipation. Figure 10 shows solutions using the unstructured meshes, in which the artificial dissipation terms are considered. It is important to observe that property oscillations are more pronounced for the solutions obtained with the unstructured meshes, even with the use of artificial dissipation, Figs. 9 (a) to (d), when compared to the solutions obtained for the structured meshes without the use of artificial dissipation, Figs. 8 (e) to (h).

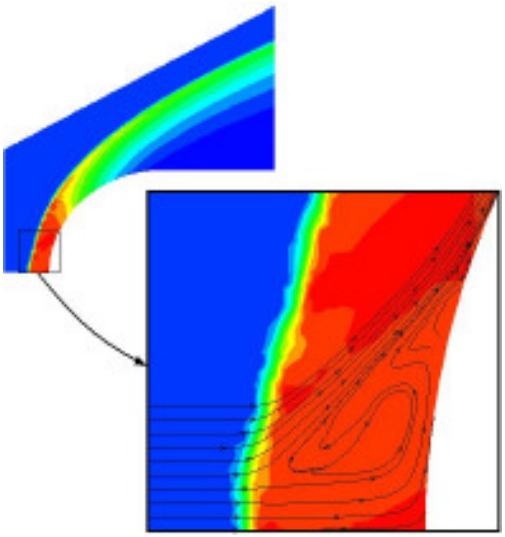

Figure 9. Details with streamtraces of the artificial recirculation observed over the triangular unstructured grid.

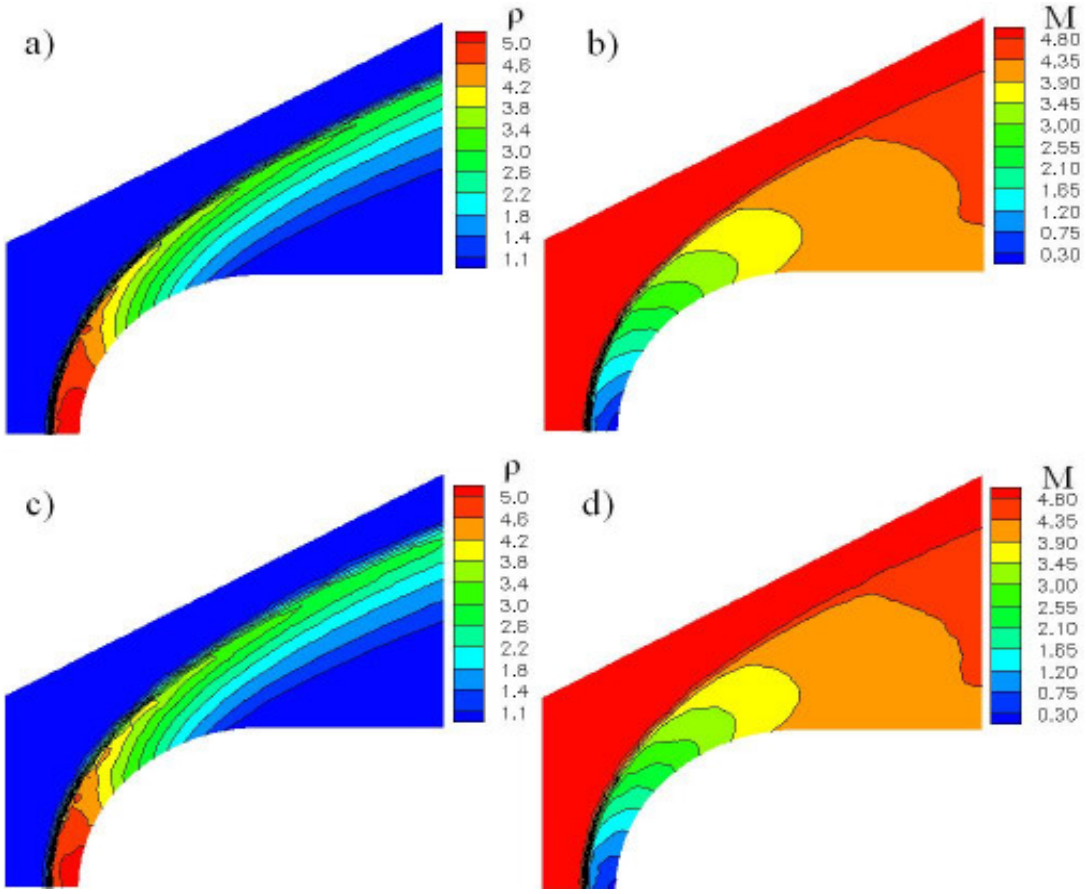

Figure 10. Density, ρ, and Mach number, M, contours: a) and b) for triangular unstructured mesh, and c) and d) for quadrilateral unstructured mesh. $M_\infty = 5$ and with the use of artificial dissipation.

5. Concluding Remarks

The present work has presented supersonic blunt body flow solutions performed using four different meshes. The objective was to address the mesh topology influence on the quality of CFD solutions. The axisymmetric Euler equations and ideal gases were considered. Liou's AUSM+ flux-vector splitting scheme, implemented in the context of a cell centered finite volume method, was used for flux computations at cell interfaces. Time march uses a fully explicit, 5-stage, Runge-Kutta time stepping scheme.

Similar solutions, assessed by the shock wave position and by the property distribution after the shock wave, were obtained for the meshes employed, except that oscillations over the field were more perceptive for the simulations performed with the triangular grid and the unstructured meshes, in opposition to the simulations over the quadrilateral grids and the structured meshes. The results indicated that the use of quadrilateral grids is preferable to triangular grids in the cases tested. Furthermore, better solutions were obtained for the quadrilateral structured meshes when compared to the quadrilateral unstructured mesh. This observation strongly suggests that the regularity and the smoothness of the mesh play an important role on the quality of the solutions. Property oscillations over the field may be led to artificial recirculations for a simulation over the triangular unstructured grid. The oscillations were considerably reduced and the appearance of the artificial recirculation was eliminated with the use of additional artificial dissipation.

It is also important to observe that property oscillations over the flowfield may create additional difficulties to implement second order accurate spatial discretization schemes, since the extrapolation of the properties from the cell center to the interfaces is based on the property values of the cell and of its neighbors. Oscillations may also jeopardize the quality of solutions when the formulation contemplates chemical reactions, even for simple geometries, since a small variation of the flow properties, as temperature, may represent a large variation in the species production rates in the kinetic reaction process.

6. Acknowledgements

The authors acknowledge Conselho Nacional de Desenvolvimento Científico e Tecnológico, CNPq, which partially supported the present research under the Integrated Project Research Grant No. 501200/2003-7

7. References

Azevedo, J. L. F., Korzenowski, H., 1998, "Comparison of Unstructured Grid Fine Volume Methods for Cold Gas Hypersonic Flow Simulations", AIAA Paper No. 98-2629, Proceedings of the 16th AIAA Applied Aerodynamics Conference, Albuquerque, NM, pp. 447-463.

ICEM CFD Engineering, 1999, ICEM CFD Tutorial Manual, Version 4.0.

Jameson, A., Schmidt, W., Turkel, E., 1981, "Numerical Solution of the Euler Equations by Finite Volume Methods Using Runge-Kutta Time-Stepping Schemes", AIAA Paper 81-1259, AIAA 14th Fluid and Plasma Dynamics Conference, Palo Alto, CA.

Jameson, A., Mavriplis, D. J., 1986, "Finite Volume Solutions of the Two-Dimensional Euler Equations on a Regular Triangular Mesh", AIAA Journal, Vol. 24, No. 4, pp. 611-618.

Liou, M.S., 1994 ,"A Continuing Search for a Near-Perfect Numerical Flux Scheme. Part I: AUSM+", NASA TM-106524, NASA Lewis Research Center, Cleveland, OH.

Liou, M.S., 1996 ,"A Sequel to AUSM: AUSM+", Journal of Computation Physics, Vol. 129, No. 2, pp. 364-382.

Lyra, P. R. M., Carvalho, D. K. E., Almeida, R. C., Feijóo, R. A., 2000, "Anisotropic Bidimensional Unstructured Mesh Generation and Adaptation for Finite Element Flow Simulation", CILAMCE.

Mavriplis, D. J., 1988, "Multigrid Solution of the Two-Dimensional Euler Equations on Unstructured Triangular Meshes," AIAA Journal, Vol. 26, No. 7, pp. 824-831.

Mavriplis, D. J., 1990, "Accurate Multigrid Solution of the Euler Equations on Unstructured and Adaptive Meshes," AIAA Journal, Vol. 28, No. 2, pp. 213-221.

Pulliam, T. H., 1986, "Artificial Dissipation Models for the Euler Equations", AIAA Journal, Vol. 24, No 12, pp. 1931-1940.

Strauss, D., and Azevedo, J. L. F., 2001, "Unstructured Multigrid Simulations of Axisymmetric Inviscid Lauch Vehicles Flows," AIAA 19th Applied Aerodynamics Conference, Anaheim, CA.